

Article

Entropy Generation of Double Diffusive Forced Convection in Porous Channels with Thick Walls and Soret Effect

Mohsen Torabi ^{1,*}, Mehrdad Torabi ² and G.P. Bud Peterson ^{1,*}

¹ The George W. Woodruff School of Mechanical Engineering, Georgia Institute of Technology, Atlanta, GA 30332, USA

² Young Researchers and Elite Club, Central Tehran Branch, Islamic Azad University, Tehran 19166, Iran; mehrdad.torabi@yahoo1.com

* Correspondence: Mohsen.Torabi@gatech.edu (M.T.); Bud.Peterson@gatech.edu (G.P.P.)

Academic Editor: Yan Jin

Received: 14 March 2017; Accepted: 13 April 2017; Published: 15 April 2017

Abstract: The second law performance of double diffusive forced convection in a horizontal porous channel with thick walls was considered. The Soret effect is included in the concentration equation and the first order chemical reaction was chosen for the concentration boundary conditions at the porous-solid walls interfaces. This investigation is focused on two principal types of boundary conditions. The first assumes a constant temperature condition at the outer surfaces of the solid walls, and the second assumes a constant heat flux at the lower wall and convection heat transfer at the upper wall. After obtaining the velocity, temperature and concentration distributions, the local and total entropy generation formulations were used to visualize the second law performance of the two cases. The results indicate that the total entropy generation rate is directly related to the lower wall thickness. Interestingly, it was observed that the total entropy generation rate for the second case reaches a minimum value, if the upper and lower wall thicknesses are chosen correctly. However, this observation was not true for the first case. These analyses can be useful for the design of microreactors and microcombustor systems when the second law analysis is taken into account.

Keywords: entropy generation; double diffusion; first order chemical reaction; porous channels; Soret effect

1. Introduction

Double diffusion convection has been observed in the ocean as a result of density stratification, which occurs when different solutes or temperature variations are present [1]. This phenomenon is of considerable interest for cases in which temperature and solute differences with different diffusivities impact the fluid motion and thermal properties of the system. Double diffusion convection has flourished into a new category of subjects when thermofluid systems with different species concentrations are being investigated [2–4]. This topic has matured into a subject with various scientific and industrial applications such as solar distillers [5,6], solar ponds [7,8], liquefied natural gas storage [9] and solidification [10].

A review of the current literature indicates an increased interest in double diffusion convection. For example, Sheremet [11] opted in favor of conjugate natural convection in a two-dimensional cavity, and later this idea was extended to an investigation for a three-dimensional cavity [12]. The walls' thicknesses were considered in both analyses [11,12]. Various illustrations, such as streamlines and concentration field, were illustrated. In a series of papers, Kefayati [8,13,14] investigates double diffusion natural convection in a cavity with various fluids and boundary conditions. While constant temperature and concentration boundary conditions were considered for

both hot and cold vertical walls of a cavity in one study [13], a magnetic field was incorporated in another study [14]. Sinusoidal boundary conditions were assumed for the temperature and concentration boundary conditions for the cold wall of the cavity [8]. The finite difference lattice Boltzmann method was used for the numerical computations, and the effect of different parameters on isoconcentrations, isotherms and streamlines were investigated [8,13,14].

Bhagat et al. [15] investigated the instability mode and flow patterns resulting from the double diffusion phenomenon in pressure driven pipe flow. This investigation considered two types of fluids in the pipe—one that served as the resident fluid, and the other one as the invading fluid. A finite-volume based software package, i.e. Gerris, was used for the solution of the transient partial differential equations that were developed to describe the double diffusion problem. The effects of the diffusivity ratio on the concentration and viscosity fields were illustrated by different contours. Nikbakhti and Rahimi [16] simulated the double diffusion convection phenomenon in a cavity with partially active side walls. The average Nusselt and Sherwood numbers were calculated for different aspect ratios and configurations, and isoconcentrations, isotherms and streamlines were plotted for various positions of the hot and cold side walls.

Alternatively, Wang et al. [17] solved the transient governing equations for double diffusion in a horizontal cavity. Soret and Dufour effects were included in the simulation, and the SIMPLE algorithm was utilized to obtain the solution. It was shown that monocellular counter-clockwise flow, monocellular clockwise flow, bicellular ascending flow and bicellular descending flow could be obtained depending on the initial conditions of the double diffusive convection. In a neatly and practical simulation, Alvarado-Juárez et al. [18] solved the steady-state two-dimensional governing differential equations for double diffusive convection in a solar still. A radiation boundary condition was considered for the top glass cover of the inclined solar distillation system. Rigorous analyses were performed to obtain the optimum values for the aspect ratio (A) and the inclination angle. The results indicate that the most suitable case for the solar still was $A = 5$ and 6.67 with an inclination angle of 20° .

Since the second law of thermodynamics can often provide more information about a system than the first law [19–21], scholars have started to re-examine double diffusion convection phenomenon in thermal systems, based on the second law of thermodynamics [22–28]. Mourad et al. [22] considered the entropy generation in a tilted cavity, with different but constant wall temperatures and concentrations. A specific control volume finite-element method was used for the solution and the total entropy generation rate was provided versus various parameters such as Grashof number, buoyancy ratio and inclination angle. By plotting the total entropy generation rate versus the inclination angles, it could be demonstrated that the total entropy generation rate may increase to a maximum amount for a specific inclination angle.

Chen and Du [23] considered the entropy generation resulting from double diffusion natural convection in a rectangular cavity. A turbulent regime was assumed for the simulation, and both local and total entropy generation rates were investigated. Somewhat later, Chen et al. [24] extended the previous mentioned study by Chen and Du [23] to the entropy generation for laminar, transient and turbulent double diffusion natural convection of Water-SiO₂ nanofluid. Similar to the investigation of Mourad et al. [22], Chen et al. [24] also showed that the buoyancy ratio could have influential impact on the total entropy generation rate and optimization of the system from a second law perspective. Most recently, Kefayati [28] extended the solution provided to a case of an open cavity [29] with entropy generation, while considering Soret and Dufour effects. A non-Newtonian power law fluid filled the cavity and a horizontal magnetic field was included in the modeling. Similar to previous investigations [8,13,14], a finite difference lattice Boltzmann method was employed, and both local and total entropy generation rates were illustrated and discussed.

Although not strongly related to the double diffusion convection, the interesting work of Matin and Khan [25] is also relevant for these situations. A microchannel was considered in which the flow was generated by electroosmotic forces and pressures, simultaneously. Velocity, temperature and concentration fields were considered, and the local and total entropy generation rates were computed and illustrated.

Later, these studies were extended to the second law analyses of double diffusion convection in porous systems [30–33]. An early study in this regard was performed by Mchirgui et al. [30] for a porous cavity with constant temperatures and concentrations for the vertical walls. This investigation [30] was later extended to that of an inclined porous cavity [31]. In both studies [30,31], transient equations were considered and the transient total and local entropy generation rates were developed. More recently, Hussain [32] opted in favor of entropy generation in a tilted sinusoidal corrugated porous enclosure. While neither the Soret nor Dufour effects were considered, an inclined magnetic field was applied on the fluid phase of the porous media. After validation, local entropy generation contours for the various cavity inclination angles were computed and illustrated.

In a somewhat similar investigation, Kefayati [33] extended the heat transfer analysis of double diffusion natural convection in a porous cavity [34] to an entropy generation investigation. Both Soret and Dufour effects were incorporated in the simulation, and a non-Newtonian power law fluid was assumed in the modeling. The study considered both non-tilted and tilted cavities, with constant temperatures and concentrations for the two side walls. In this investigation [33], the total entropy generation versus the power law index was illustrated for different values of the Rayleigh and Darcy numbers. It was shown that depending on the parametric values of the system, the maximum or minimum values for the total entropy generation rate or Bejan number could be determined.

The main objective of the current investigation is to extend the double diffusion convection phenomenon in porous channels. An extensive literature review revealed no investigation evaluating double diffusive convection for a pressure driven flow within a porous channel. As a result, solid upper and lower walls were incorporated in the simulation [20,35,36], and both magnetic and radiation field effects were considered in the modeling. The following section provides the details of the problem investigated, with mathematical illustrations for the fundamental equations. Section 3 presents the solution methodology and comprehensively examines the illustrated plots resulting from the sample mathematical calculations. Finally, Section 4 summarizes the most important findings and presents suggestions for further investigation in this area.

2. Problem Statement

A horizontal porous channel similar to that shown in Figure 1 was considered, where the upper and lower channel walls' thicknesses were varied in relationship to the height of the channel [35,37]. Similar to other recent investigations [35,36], two cases were considered. In the first case, the upper cooler wall and warmer lower wall temperatures were held constant. In the second case a constant heat flux was applied to the lower wall and a convection heat transfer condition was applied to the upper wall. First order chemical reaction boundary conditions were assumed for both the inner wall porous material interfaces [38–40]. The current analysis employed classical no-slip boundary conditions for both velocity and temperature [20]. A similar geometry has been recently considered for heat and mass transfer analysis [20,36], although the concentration equations and radiation term have not been included. Therefore, the detailed mathematical analyses have been provided within the Appendix for interested readers. By using the relevant dimensionless parameters the governing non-dimensionalized differential equations of the problem take the following form:

Momentum

$$1 + \frac{1}{\varepsilon} \frac{d^2 U}{dY^2} - \frac{U}{Da} - M^2 U = 0 \quad Y_1 < Y \leq Y_2 \quad (1)$$

Energy

$$\frac{d}{dY} \left[\frac{d\theta_1}{dY} \right] + Q_1 = 0 \quad 0 < Y \leq Y_1 \quad (2a)$$

$$\frac{d^2 \theta_p}{dY^2} + \frac{\text{Pr Ec}}{Da} U^2 + \text{Pr Ec} \left(\frac{dU}{dY} \right)^2 + M^2 \text{Pr Ec} U^2 + Q_p + Rd \frac{d^2 \theta_p}{dY^2} = 0 \quad Y_1 < Y \leq Y_2 \quad (2b)$$

$$\frac{d}{dY} \left[\frac{d\theta_2}{dY} \right] + Q_2 = 0 \quad Y_2 \leq Y < 1 \tag{2c}$$

Concentration

$$\frac{d^2\phi}{dY^2} + Sr \frac{d^2\theta_p}{dY^2} = 0 \quad Y_1 \leq Y < Y_2 \tag{3}$$

with the following outer and inner boundary conditions:

Case one

$$Y = 0 \quad \theta_1 = \theta_H \tag{4a}$$

$$Y = 1 \quad \theta_2 = 1 \tag{4b}$$

Case two

$$Y = 0 \quad -\frac{d\theta_1}{dY} = Q_H \tag{5a}$$

$$Y = 1 \quad -\frac{d\theta_2}{dY} = Nc(\theta_2 - 1) \tag{5b}$$

Both cases:

$$Y = Y_1 \quad U = 0 \quad \theta_1 = \theta_p \quad \left. \frac{d\theta_1}{dY} \right|_{Y=Y_1} = k_{e1} \left. \frac{d\theta_p}{dY} \right|_{Y=Y_1} \quad \left. \frac{d\phi}{dY} \right|_{Y=Y_1} = -\gamma\phi \tag{6a}$$

$$Y = Y_2 \quad U = 0 \quad \theta_2 = \theta_p \quad \left. \frac{d\theta_2}{dY} \right|_{Y=Y_2} = k_{e2} \left. \frac{d\theta_p}{dY} \right|_{Y=Y_2} \quad \left. \frac{d\phi}{dY} \right|_{Y=Y_2} = \gamma\phi \tag{6b}$$

where in Equation (2b) the $Pr \times Ec = Br$, the Brinkman number. Consequently, the following dimensionless form of the local entropy generation rate governs the second law perspective of the investigated thermal system:

$$N_s = \frac{\dot{S}^m h_3^2}{k_1} = \begin{cases} \frac{1}{\theta_1^2} \left(\frac{d\theta_1}{dY} \right)^2 & 0 < Y < Y_1 \\ \frac{k_{e1}}{\theta_p^2} \left(\frac{d\theta_p}{dY} \right)^2 + \frac{k_{e1} Pr Ec}{Da\theta_p} U^2 + \frac{k_{e1} Pr Ec}{\theta_p} \left(\frac{dU}{dY} \right)^2 & Y_1 < Y < Y_2 \\ + \frac{k_{e1} M^2 Pr Ec}{\theta_p} U^2 + \phi_1 \left[\frac{1}{\phi} \left(\frac{d\phi}{dY} \right)^2 + \frac{1}{\theta_p} \left(\frac{d\phi}{dY} \right) \left(\frac{d\theta_p}{dY} \right) \right] & \\ \frac{k_{e1}}{k_{e2} \theta_2^2} \left(\frac{d\theta_2}{dY} \right)^2 & Y_2 < Y < 1 \end{cases} \tag{7}$$

Integration to obtain the total entropy generation rate can be found as

$$N_t = \int_0^1 N_s dY \tag{8}$$

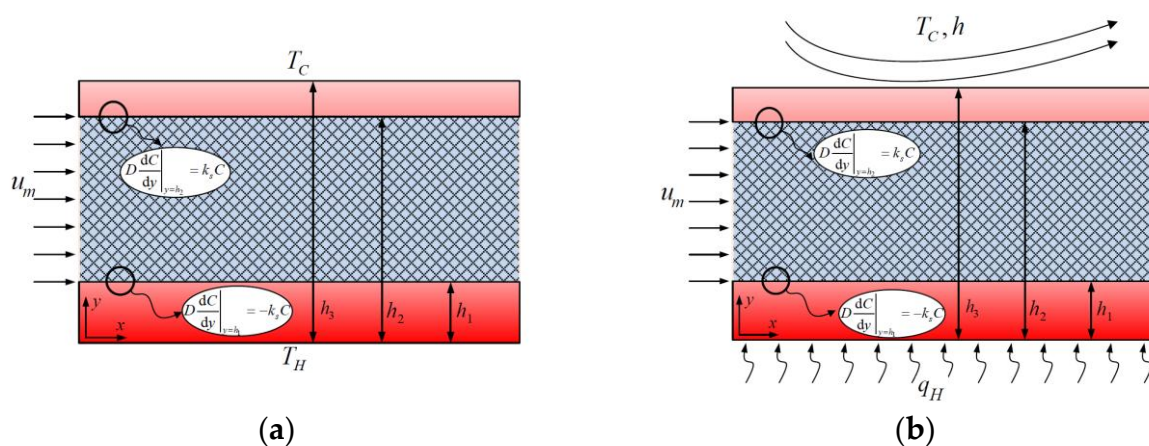


Figure 1. Configuration of the microchannels filled with a porous material; (a) Case one, (b) Case two.

3. Results and Discussion

The solution procedure is similar to that of recent publications by Torabi and co-workers [20,36]. First the velocity distribution is obtained, and is digested in the energy differential Equation (2b). After obtaining the temperature field, it is incorporated into the concentration Equation (3) to obtain the species concentration. Finally, velocity, temperature and species fields are used to obtain entropy generation by using Equation (7). It is useful to note that the constant parameters for velocity distribution are obtained completely analytically, while the constant parameters for temperature distribution and concentration fields are obtained numerically, case-by case. Interested readers may find detailed solution procedure in recently published articles in this area [20,36]. This solution methodology has been validated against completely analytical solution procedure for various problems and has been observed to be very accurate [41,42]. Although this section focuses primarily on the total entropy generation rate, a few sample analyses regarding the effects of radiation parameter on the temperature and radiation, Soret and Damkohler parameters on the local entropy generation rate are provided. Hence, this section is divided into two subsections: Subsection 3.1 which contains temperature and local entropy generation plots; and Subsection 3.2 which includes the total entropy generation rate plots. *In all illustrated calculations in this investigation, except Figure 7 which is about the influence of boundary conditions, part a of each figure is related to the first case and part b of the same figure is about the impact of the same parameter on the second case.*

3.1. Temperature and Local Entropy Generation Rate

Figure 2 illustrates the effects of the radiation parameter on the temperature distribution for both cases. As illustrated, the radiation parameter increases the rate of heat transfer and consequently decreases the temperature within the system. The influence of the radiation increases significantly when the power changes from zero to unity, although it does not significantly influence the temperature when the power changes to two from unity. The reduction in the temperature has been examined by including the radiation effect in the system as it has been reported by previous scholars [43]. As the temperature boundary conditions for the first case are fixed and for the second case are not fixed in this investigation, the variation of any parameter is more likely to impact the temperature field of the second case rather than the first one. This consequently controls the behavior of the total entropy generation rate versus other parameters in case one and two, which will be discussed in the next subsection. Figure 3, which serves as a companion to Figure 2, visualizes the radiative effects on the entropy generation rate. Although the effect of radiative heat transfer on the temperature distribution can be seen more clearly for the second case in Figure 2, Figure 3 shows that the radiative effect on the entropy generation rate is more prominent for the first case compared with the second one. This is an important result, which highlights the importance of the second law analyses for these types of systems.

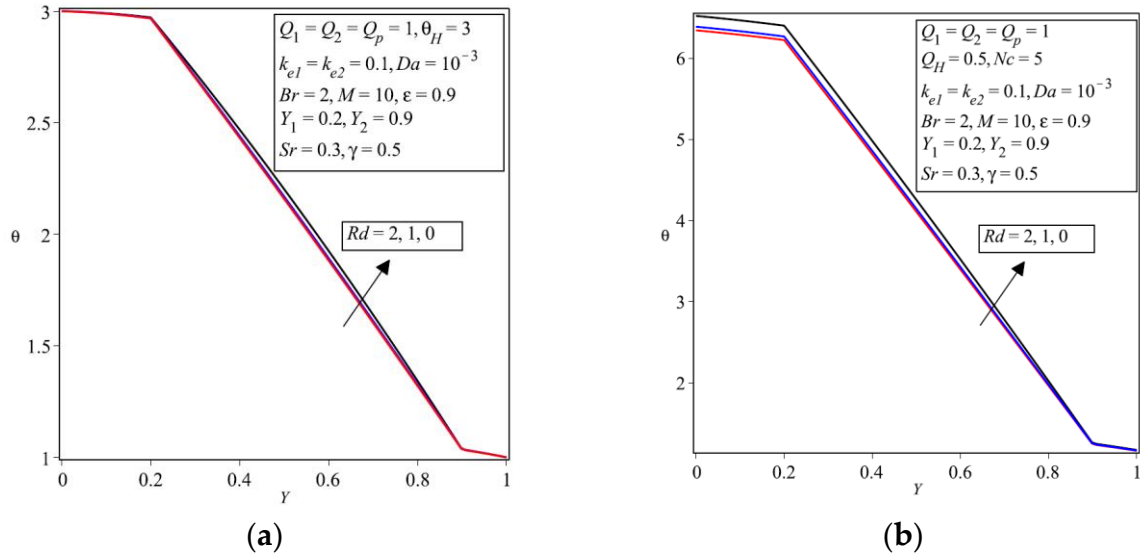


Figure 2. Effect of radiation parameter on the temperature distribution in the porous channels.

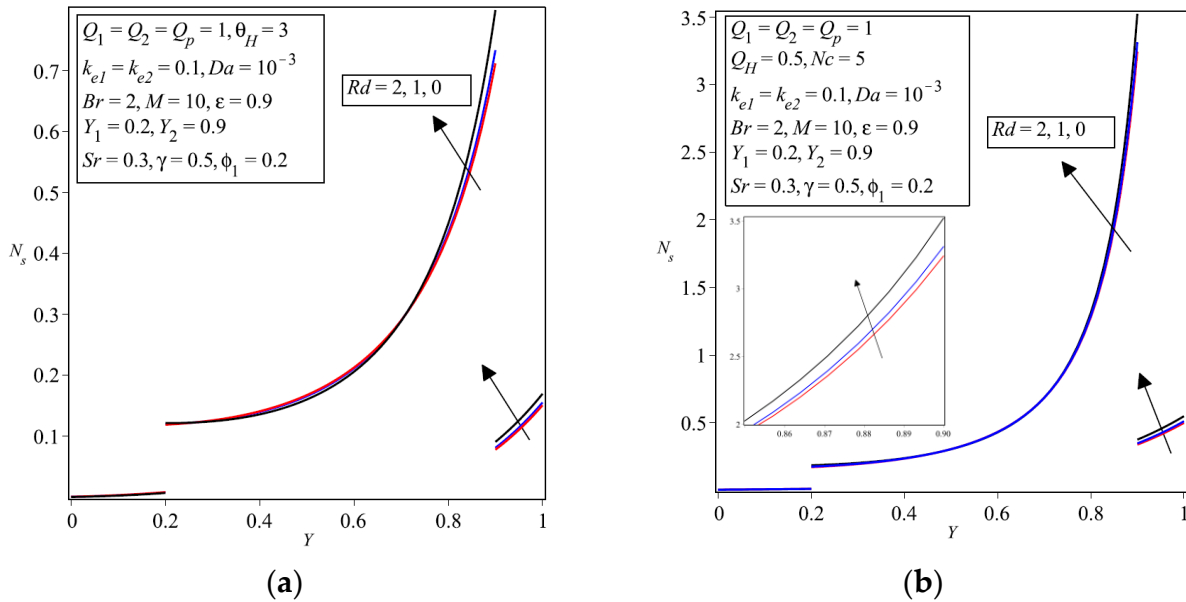


Figure 3. Effect of radiation parameter on the local entropy generation rate in the porous channels.

The effect of the Soret number, which describes the temperature effects on the concentration distribution, on the local entropy generation rate has been illustrated in Figure 4. Consequently, Figure 5 depicts the effect of Damkohler parameter, which describes the ratio of chemical reaction to diffusion, on the local entropy generation rate. From both figures, it is clearly seen that these parameters have strong effect on the local entropy generation of the first case, although their effect on the second case is marginal. Moreover, depending on the location of the probed point in the channel, Soret and Damkohler parameters may have increasing or decreasing effects on the local entropy generation rate, as it is seen from Figures 4 and 5.

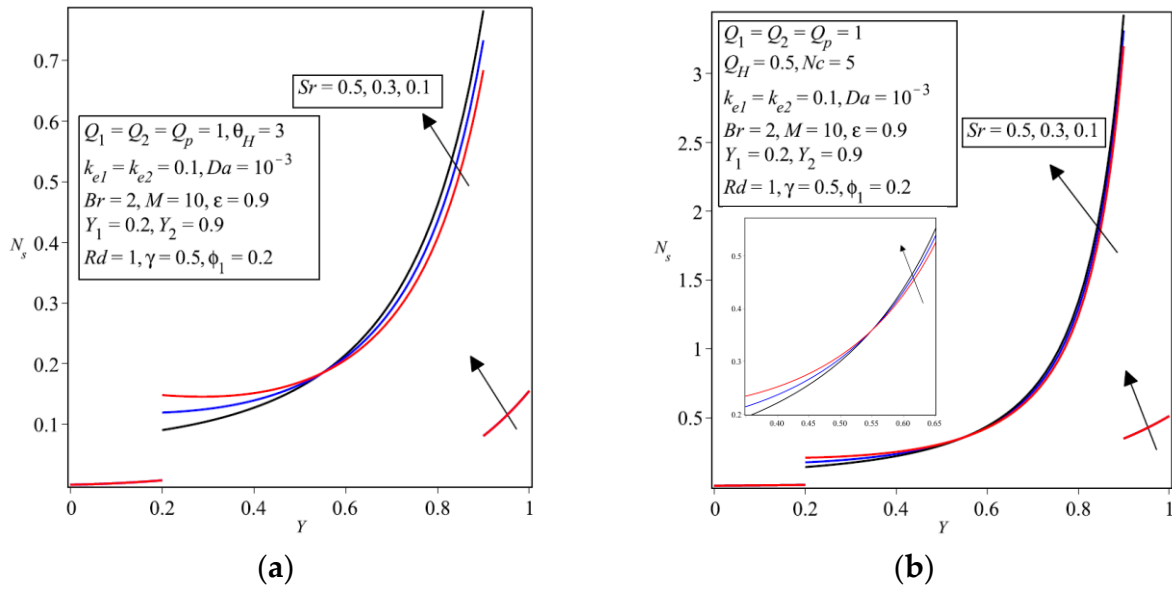


Figure 4. Effect of Soret parameter on the local entropy generation rate in the porous channels.

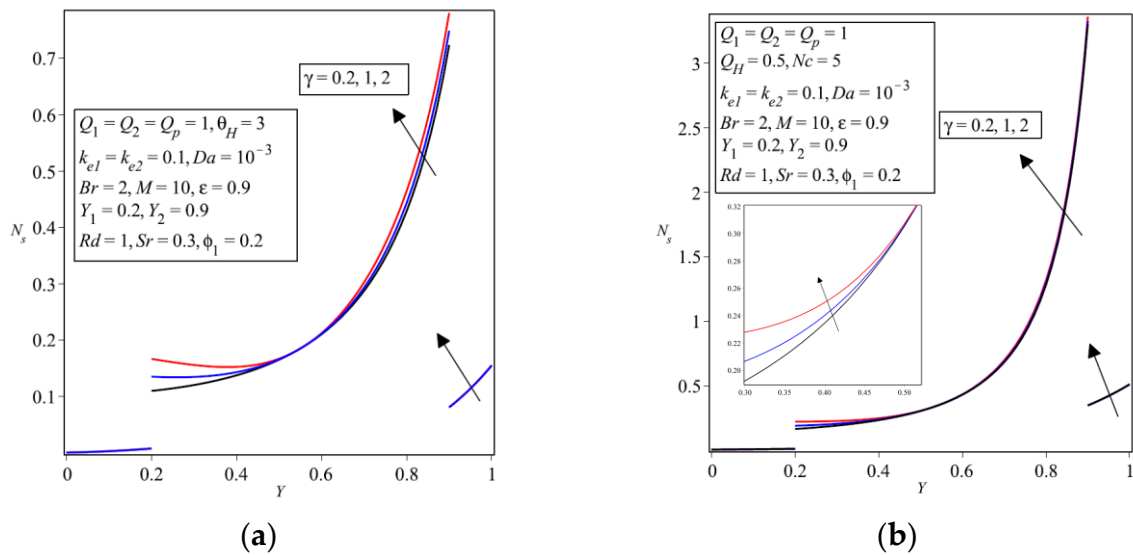


Figure 5. Effect of Damkohler parameter on the local entropy generation rate in the porous channels.

3.2. Total Entropy Generation Rate

Figure 6 plots the variation of the total entropy generation rate versus radiation parameter using various values for Soret effect. Similar to the effect of radiation parameter on the temperature, the total entropy generation rate decreases sharply by increasing the radiation effect from zero to unity, and then it continues to decrease with a lesser slope. Unlike the effect of Soret parameter on the local entropy generation rate, the effect of Soret parameter on the total entropy generation rate for both cases is significant. As can be seen from Figure 6a,b, the Soret effect tends to decrease the total entropy generation rate for both cases. While the effects of both Soret and radiation parameters for the first case are on the third order of decimal, these effects for the second case affect the total entropy generation by the first order of decimal. This can be attributed to the fact that the temperature boundary conditions for the second case are not fixed, and changing the parametric values of the system may have stronger effects of the temperature compared to the first case (For example see Figure 2). These modifications on the temperature impact the local entropy generation of the second case more than the first case, and consequently the total entropy generation for the second case seems to be more sensible to these parameters. Figure 7 illustrates the variation of the total entropy

generation rate versus the Damkohler parameter for various values of dimensionless parameters related to the outer boundary conditions for both cases. It is observed from this figure that the Damkohler parameter slightly increases the total entropy generation rate as it has been increased from almost zero to two. Effects of other boundary related parameters such as the temperature of the hot lower wall for the first case, and the heat flux and convection parameters for the second case, both on the total entropy generation, are similar to the recent investigation reported in Reference [35], and will not be discussed here.

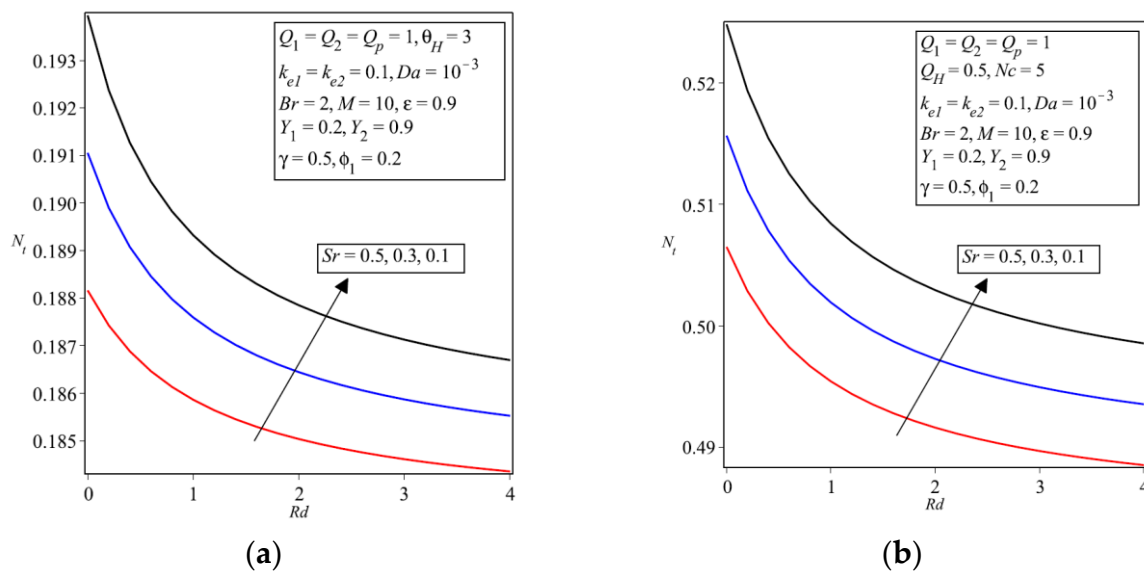
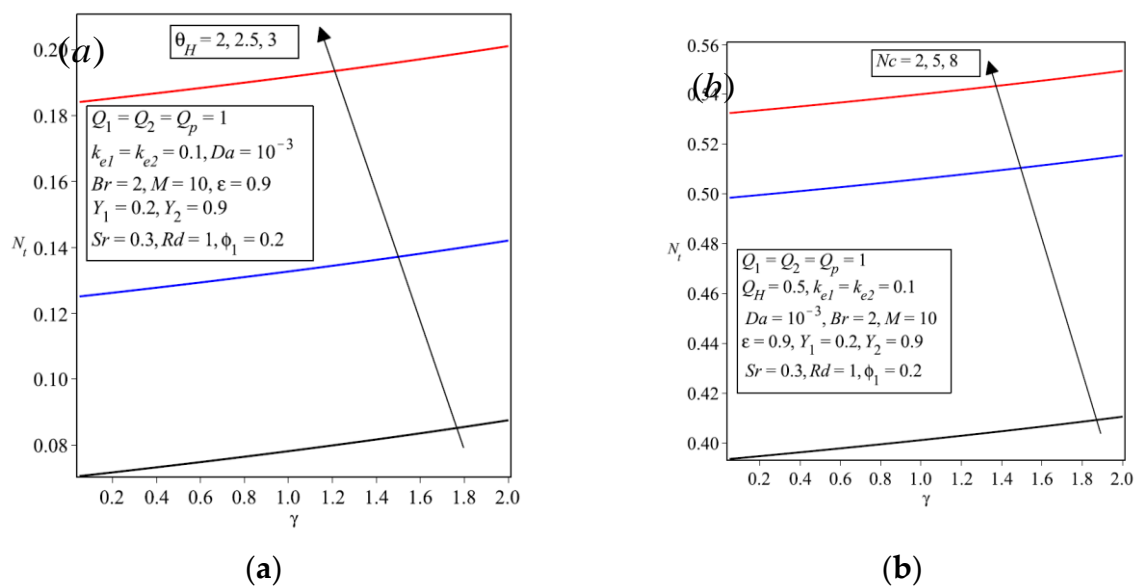


Figure 6. Variation of the total entropy generation rate versus radiation parameter with various values for Soret parameters.



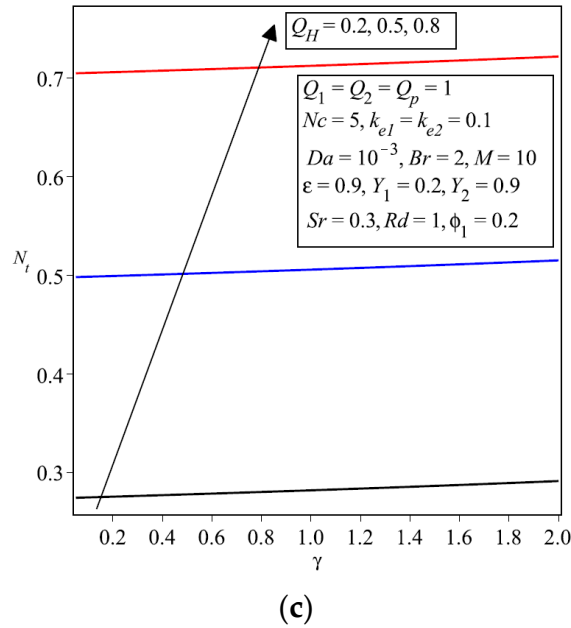


Figure 7. Variation of the total entropy generation rate versus Damkohler parameter with various values for (a) hot wall temperature, (b) convection coefficient and (c) heat flux.

When examining a thermophysical system, the thermal properties of the materials, along with the configuration properties of the system can significantly impact the optimum performance for the system. For the system under investigation here, it is possible to try to achieve the best configuration by varying the walls' thicknesses and looking for an optimum second law performance of the system. Figures 8–11 are devoted to illustrate the total entropy generation rate as a function of the wall thicknesses using various values for other parameters and possibly finding the optimum configuration of the system. Generally speaking, as mentioned before, due to the fixed temperature boundary conditions for the first case and non-fixed temperature boundary conditions for the second case, the fluctuation of the total entropy generation for the second case with respect to various parameters should be more than the fluctuations for the first case total entropy generation. These fluctuations help researchers to find an optimum condition for the second law performance of the system under investigation.

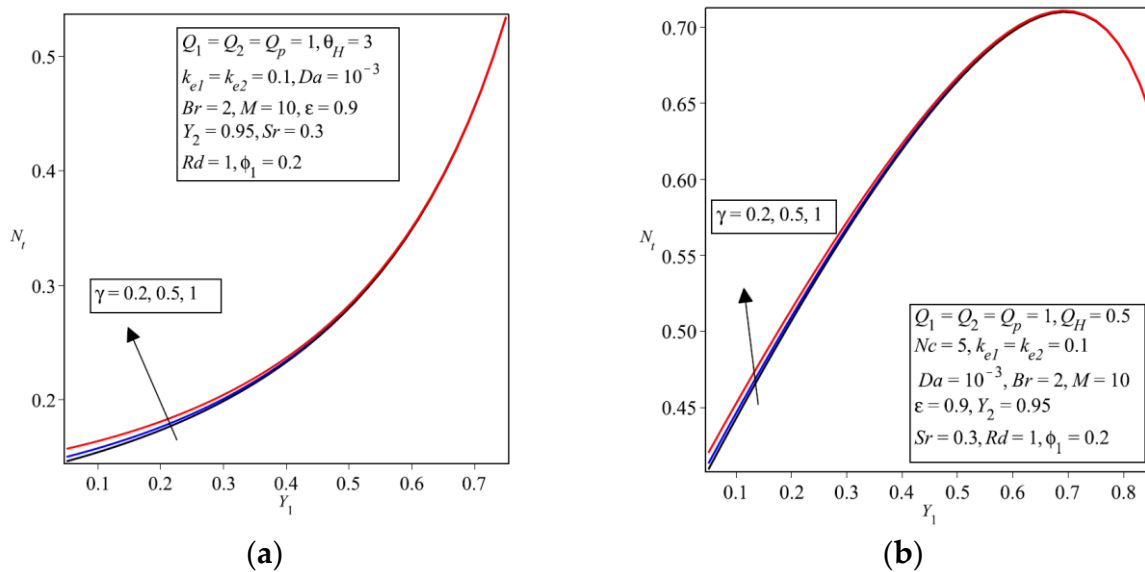


Figure 8. Variation of the total entropy generation rate versus lower wall's thickness with various values for Damkohler parameter.

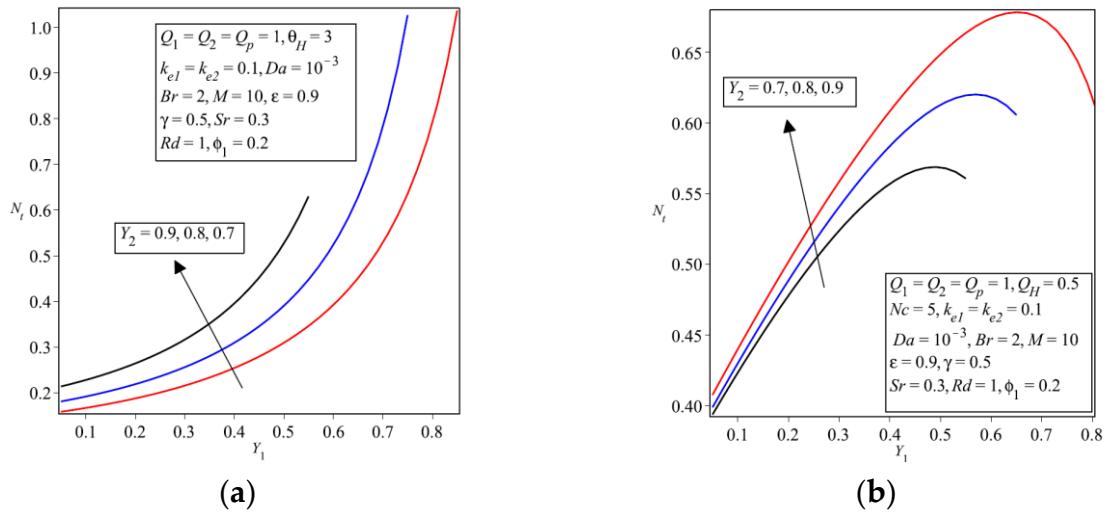


Figure 9. Variation of the total entropy generation rate versus lower wall's thickness with various values for Y_2 .

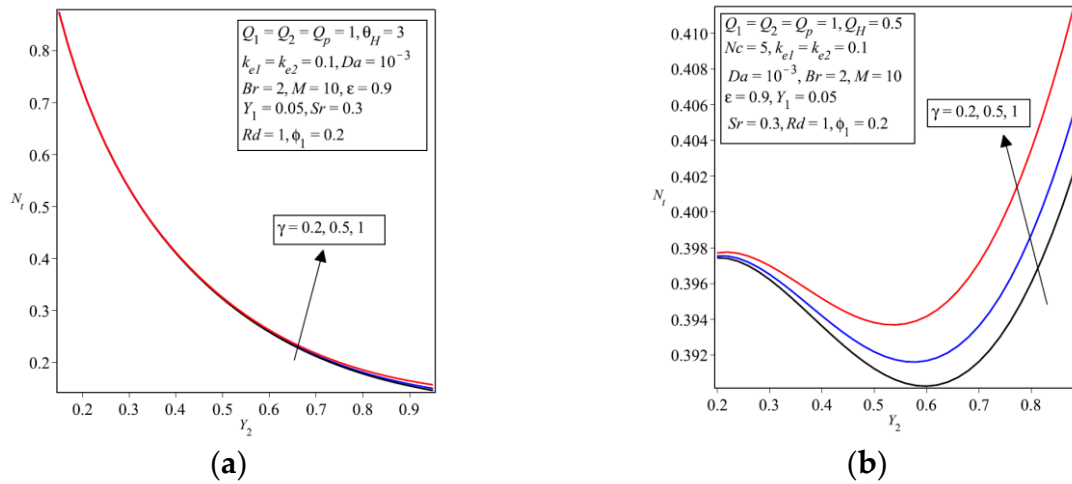


Figure 10. Variation of the total entropy generation rate versus Y_2 with various values for Damkohler parameter.

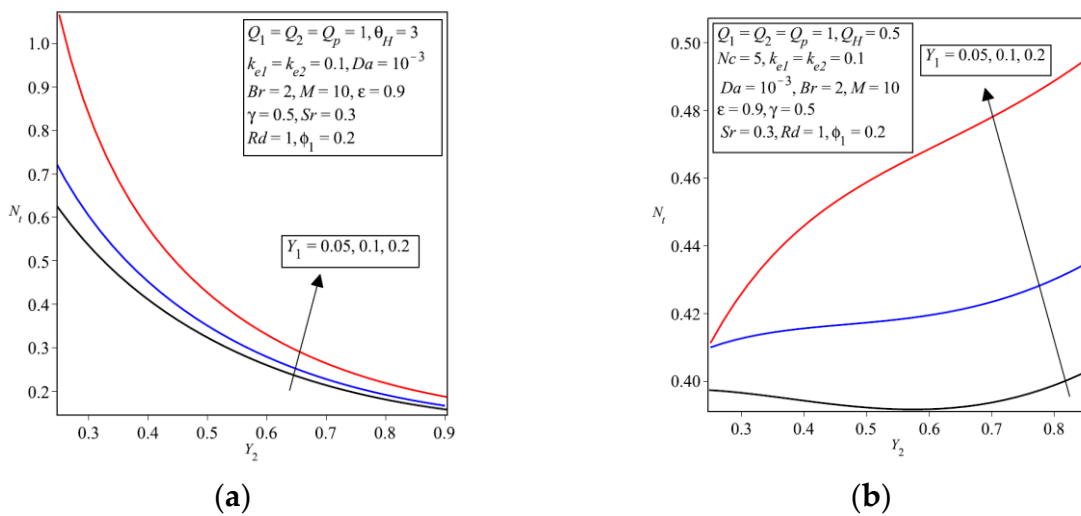


Figure 11. Variation of the total entropy generation rate versus Y_2 with various values for the lower wall's thickness.

Figure 8 shows that while the total entropy generation rate versus the lower wall thickness is always increasing for the first case, this behavior may change when dealing with the second case. For the second case, when the value for γ_2 is fixed at 0.95, the total entropy generation rate versus the lower wall thickness increases at first, reaches a maxima and then starts to decrease, as illustrated in Figure 8b. Similar behavior for both cases is seen when other values for γ_2 are chosen, which is illustrated in Figure 9. Figure 9b shows the relationship between the thickness of the porous section of the channel, i.e. the smaller the value of γ_2 , the lower would be the maximum value of the total entropy generation rate, which the second case experiences. Figures 10 and 11 represent the total entropy generation rate versus γ_2 for different values of the Damkohler parameter and the lower wall thickness, respectively. It is apparent from Figures 10a and 11a that the variation of the total entropy generation rate with γ_2 for the first cases is always decreasing. This, again, can be justified by the fixed temperature boundary conditions for this case, which does not give enough room to the temperature profile of the system to vary, and hence the behavior of the total entropy generation may not vary significantly. However, as shown in Figures 10b and 11b, it may be possible to find an optimum value for γ_2 that decreases the total entropy generation rate to a minimum value for the second case, and hence the exergy destruction of the system would be minimized. As shown in Figure 10b, when the value of γ_1 is fixed at 0.05, the total entropy generation rate versus γ_2 first slightly increases and then starts to decrease reaching a minimum value and finally continuously increases as γ_2 increases. However, when the Damkohler parameter is fixed at 0.5 and the value of γ_1 is increased to 0.1 or 0.2 in Figure 11b, the minimum point is no longer apparent and the behaviour of the total entropy generation rate versus γ_2 is continuously increasing.

4. Conclusions

Two types of horizontal porous channels are considered in this investigation to examine the entropy generation of double diffusion forced convection systems. A first order chemical reaction boundary condition was used for the interfaces of the porous material with solid walls, and the Soret effect was included in the modeling. The radiation effect and a constant magnetic field were also considered in the formulation. It was found that although radiation, Soret and Damkohler parameters have marginal effects on the temperature distribution and the local entropy generation rate, their effects on the total entropy generation rate for both cases are non-negligible. Throughout the investigations it was shown that the effects of radiation and Soret numbers for the first case is on the third order of decimal, while these effects impact the second decimal of the total entropy generation for the second case. Hence, it was concluded that these parameters affect the second case more drastically than the first case. It was also observed that for the first case, i.e. constant temperature boundary conditions, the total entropy generation rate versus γ_1 or γ_2 may be always increasing or decreasing. However, the second case resulted in a considerably more complicated relationship. This is attributed mainly to the fixed temperature boundary conditions for the first case, and non-fixed temperature boundary condition for the second case. As discussed, for the parametric values examined in this investigation, the total entropy generation rate versus the lower wall's thickness always reaches a maximum point. Also, the total entropy generation rate versus γ_2 may or may not have a minimum value depending on the value of the lower wall thickness. Again, as the temperature boundaries at the second case has more room to vary, they impact the flexible variation of the temperature and finally the total entropy generation for this case can have more extremum points compared with the first case. These findings are crucial for microreactors or microcombustor systems where the optimum second law performance is the design target. Using the analyses developed in this investigation, it is possible to optimize the configuration of the system and, as a result, to minimize the exergy destruction.

Author Contributions: Mo. Torabi and Me. Torabi contributed to the solution of the equations and illustrations. G.P. Peterson supported this investigation by his comments and advised about the presentation of the results and various technical English proofreading.

Conflicts of Interest: The authors declare no conflict of interest.

Nomenclature

B_0	magnetic field, T
Br	Brinkman number ($Pr \cdot Ec$)
Da	Darcy number
Ec	Eckert number
h	convection heat transfer (Case two), $W \cdot m^{-2} \cdot K^{-1}$
h_3	height of the channel, m
k_1	reference thermal conductivity for lower solid material, $W \cdot m^{-1} \cdot K^{-1}$
k_2	reference thermal conductivity for upper solid material, $W \cdot m^{-1} \cdot K^{-1}$
k_{eff}	effective thermal conductivity of porous medium, $W \cdot m^{-1} \cdot K^{-1}$
k_{e1}	ratio of porous medium thermal conductivity to lower solid material thermal conductivity
k_{e2}	ratio of porous medium thermal conductivity to upper solid material thermal conductivity
N_s	dimensionless local entropy generation rate
Nc	dimensionless convection heat transfer (Case two)
M	Hartmann number
Pr	Prandtl number
Q_1	dimensionless volumetric internal heat generation rate for the lower solid material
Q_2	dimensionless volumetric internal heat generation rate for the upper solid material
Q_H	dimensionless heat flux boundary condition (Case two)
Q_p	dimensionless volumetric internal heat generation rate for the porous medium
\dot{q}_1	volumetric internal heat generation rate for the lower solid material, $W \cdot m^{-3}$
\dot{q}_2	volumetric internal heat generation rate for the upper solid material, $W \cdot m^{-3}$
q_H	heat flux boundary condition (Case two), $W \cdot m^{-2}$
\dot{q}_p	volumetric internal heat generation rate for the porous medium, $W \cdot m^{-3}$
Rd	dimensionless radiation parameter
\dot{s}''	local entropy generation rate, $W \cdot m^{-3} \cdot K^{-1}$
T	temperature, K
T_1	temperature of the lower solid material, K
T_2	temperature of the upper solid material, K
T_c	outer temperature of the upper solid material, K
T_H	inner temperature of the lower solid material, K
T_p	temperature of the porous medium, K
U	dimensionless velocity
u	velocity of the fluid in porous medium, $m \cdot s^{-1}$
u_r	characteristics velocity
Greek symbols	
κ	permeability, m^2
κ^*	Rosseland mean absorption coefficient
ε	porosity
μ_f	dynamic viscosity of the base fluid, $Kg \cdot s^{-1} \cdot m^{-1}$
θ	dimensionless temperature
θ_1	dimensionless temperature of the lower solid material
θ_2	dimensionless temperature of the upper solid material
θ_p	dimensionless temperature of the porous medium
θ_H	dimensionless temperature at outer side of the lower wall
σ	electrical conductivity of fluid, $S \cdot m^{-1}$
σ^*	Stefan-Boltzmann constant, $W \cdot m^{-2} \cdot K^{-4}$

Appendix

As shown in Figure 1 two types of horizontal porous channels are considered in this investigation. The fluid flow was assumed to be under influence of a constant magnetic field, and the

effect of thermal radiation was considered in the porous section of the system. By assuming the above outlined conditions, the momentum, energy and concentration governing equations of the problem can be expressed as [20,35,36]:

Momentum

$$-\frac{\partial p}{\partial x} + \frac{\mu_f}{\varepsilon} \frac{d^2 u}{dy^2} - \frac{\mu_f}{\kappa} u - \sigma B_0^2 u = 0 \quad h_1 \leq y < h_2 \quad (\text{A1})$$

Energy

$$k_1 \frac{d}{dy} \left[\frac{dT_1}{dy} \right] + \dot{q}_1 = 0 \quad 0 < y \leq h_1 \quad (\text{A2a})$$

$$k_{\text{eff}} \frac{d^2 T_p}{dy^2} + \frac{\mu_f}{\kappa} u^2 + \mu_f \left(\frac{du}{dy} \right)^2 + \sigma B_0^2 u^2 - \frac{\partial q_r}{\partial y} + \dot{q}_p = 0 \quad h_1 \leq y < h_2 \quad (\text{A2b})$$

$$k_2 \frac{d}{dy} \left[\frac{dT_2}{dy} \right] + \dot{q}_2 = 0 \quad h_2 < y \leq h_3 \quad (\text{A2b})$$

Concentration

$$D \frac{d^2 C}{dy^2} + D_r \frac{d^2 T_p}{dy^2} = 0 \quad h_1 \leq y < h_2 \quad (\text{A3})$$

The radiation parameter takes the form

$$q_r = \frac{-4\sigma^*}{3\kappa^*} \frac{dT_p^4}{dy} \quad (\text{A4})$$

and using a Rosseland approximation, the last term of the energy equation in the porous section of the channel is transformed to

$$\frac{\partial q_r}{\partial y} = \frac{-16\sigma^* T_0^3}{3\kappa^*} \frac{d^2 T_p}{dy^2} \quad (\text{A5})$$

Hence, Equation (A2b) reads:

$$k_{\text{eff}} \frac{d^2 T_p}{dy^2} + \frac{\mu_f}{\kappa} u^2 + \mu_f \left(\frac{du}{dy} \right)^2 + \sigma B_0^2 u^2 + \frac{16\sigma^* T_0^3}{3\kappa^*} \frac{d^2 T_p}{dy^2} + \dot{q}_p = 0 \quad h_1 \leq y < h_2 \quad (\text{A6})$$

The outer thermal boundary conditions of the system for each case are:

Case one

$$y = 0 \quad T_1 = T_H \quad (\text{A7a})$$

$$y = h_3 \quad T_2 = T_C \quad (\text{A7b})$$

Case two

$$y = 0 \quad -k_1 \frac{dT_1}{dy} = q_H \quad (\text{A8a})$$

$$y = h_3 \quad -k_2 \frac{dT_2}{dy} = h(T_2 - T_C) \quad (\text{A8b})$$

The inner boundary conditions for both cases under investigation are:

$$y = h_1 \quad u_p = 0 \quad T_1 = T_p \quad k_1 \frac{dT_1}{dy} \Big|_{y=h_1} = k_{\text{eff}} \frac{dT_p}{dy} \Big|_{y=h_1} \quad D \frac{dC}{dy} \Big|_{y=h_1} = -k_s C \quad (\text{A9a})$$

$$y = h_2 \quad u_p = 0 \quad T_2 = T_p \quad k_2 \left. \frac{dT_2}{dy} \right|_{y=h_2} = k_{eff} \left. \frac{dT_p}{dy} \right|_{y=h_2} \quad D \left. \frac{dC}{dy} \right|_{y=h_2} = k_s C \quad (A9b)$$

The entropy generation rate in the considered system consists of entropy generation due to the heat transfer through walls and porous section of the channel, entropy generation due to the fluid friction, entropy generation due to the magnetic field and entropy generation due to the mass transfer resulting from the concentration equation. Incorporating the various aspects of the entropy generation rate, the formulation for the local entropy generation rate can be expressed as:

$$\dot{S}'' = \begin{cases} \frac{k_1}{T_1^2} \left(\frac{dT_1}{dy} \right)^2 & 0 < y < h_1 \\ \frac{k_{eff}}{T_p^2} \left(\frac{dT_p}{dy} \right)^2 + \frac{\mu_f}{T_p} \left(\frac{du}{dy} \right)^2 + \frac{\mu_f}{\kappa T_p} u^2 + \frac{\sigma B_0^2}{T_p} u^2 + \frac{RD}{C} \left(\frac{dC}{dy} \right)^2 + \frac{RD}{T_p} \left(\frac{dC}{dy} \right) \left(\frac{dT_p}{dy} \right) & h_1 < y < h_2 \\ \frac{k_2}{T_2^2} \left(\frac{dT_2}{dy} \right)^2 & h_2 < y < h_3 \end{cases} \quad (A10)$$

Finally, the total entropy generation rate is given by integrating over the height of the channel for the local entropy generation rate. To provide the universal data, the above mentioned governing equations have to be non-dimensionalized. By considering $u_r = -\frac{h_3^2}{\mu_f} \frac{\partial p}{\partial x}$ and then introducing the following dimensionless parameters:

$$\begin{aligned} \theta_1 &= \frac{T_1}{T_c} & \theta_p &= \frac{T_p}{T_c} & \theta_2 &= \frac{T_2}{T_c} & \theta_H &= \frac{T_H}{T_c} & Y &= \frac{y}{h_3} & Y_1 &= \frac{h_1}{h_3} & Y_2 &= \frac{h_2}{h_3} \\ Q_1 &= \frac{\dot{q}_1 h_3^2}{k_1 T_c} & Q_2 &= \frac{\dot{q}_2 h_3^2}{k_2 T_c} & Q_p &= \frac{\dot{q}_p h_3^2}{k_{eff} T_c} & Q_H &= \frac{q_H h_3}{k_1 T_c} & U &= \frac{u}{u_r} & \phi &= \frac{C}{C_0} \\ Da &= \frac{\kappa}{h_3^2} & Ec &= \frac{u_r^2}{C_p T_c} & Pr &= \frac{\mu_f C_p}{k_{eff}} & M &= \sqrt{\frac{\sigma}{\mu_f}} h_3 B_0 & k_{e1} &= \frac{k_{eff}}{k_1} & k_{e2} &= \frac{k_{eff}}{k_2} \\ Nc &= \frac{h h_3}{k_2} & Sr &= \frac{D_r T_c}{DC_0} & \gamma &= \frac{k_1 h_3}{D} & Rd &= \frac{16 \sigma^* T_0^3}{3 \kappa^* k_{eff}} & \phi_1 &= \frac{RDC_0}{k_1} \end{aligned} \quad (A11)$$

The system of equations are easily transformed to dimensionless partial differential equations which has been provided in Section 2. As mentioned before, the solution procedure is similar to that of recent publications by Torabi and co-workers [20,36], and is not repeated here for the sake of brevity.

References

1. Stommel, H.; Arons, A.B.; Blanchard, D. An oceanographical curiosity: The perpetual salt fountain. *Deep Sea Res.* **1956**, *3*, 152–153.
2. Zambra, C.E.; Moraga, N.O.; Escudey, M. Heat and mass transfer in unsaturated porous media: Moisture effects in compost piles self-heating. *Int. J. Heat Mass Transf.* **2011**, *54*, 2801–2810.
3. Patil, P.M.; Roy, S.; Momoniat, E. Thermal diffusion and diffusion-thermo effects on mixed convection from an exponentially impermeable stretching surface. *Int. J. Heat Mass Transf.* **2016**, *100*, 482–489.
4. Hidouri, N.; Bouabid, M.; Magherbi, M.; Brahim, A. Ben Effects of radiation heat transfer on entropy generation at thermosolutal convection in a square cavity subjected to a magnetic field. *Entropy* **2011**, *13*, 1992–2012.
5. Ghachem, K.; Kolsi, L.; Maatki, C.; Hussein, A.K.; Borjini, M.N. Numerical simulation of three-dimensional double diffusive free convection flow and irreversibility studies in a solar distiller. *Int. Commun. Heat Mass Transf.* **2012**, *39*, 869–876.
6. Alvarado-Juárez, R.; Álvarez, G.; Xamán, J.; Hernández-López, I. Numerical study of conjugate heat and mass transfer in a solar still device. *Desalination* **2013**, *325*, 84–94.
7. Karim, C.; Slim, Z.; Kais, C.; Jomâa, S.M.; Akbarzadeh, A. Experimental study of the salt gradient solar pond stability. *Sol. Energy* **2010**, *84*, 24–31.
8. Kefayati, G.R. Mesoscopic simulation of double-diffusive mixed convection of Pseudoplastic Fluids in an enclosure with sinusoidal boundary conditions. *Comput. Fluids* **2014**, *97*, 94–109.

9. Okorafor, A.A.; He, S.; Morrison, D. Experimental investigation of three-dimensional flow in a double-diffusive interface system with lateral heating. *Exp. Therm. Fluid Sci.* **2012**, *42*, 143–153.
10. Ghenai, C.; Mudunuri, A.; Lin, C.X.; Ebadian, M.A. Double-diffusive convection during solidification of a metal analog system (NH₄Cl-H₂O) in a differentially heated cavity. *Exp. Therm. Fluid Sci.* **2003**, *28*, 23–35.
11. Sheremet, M.A. The influence of cross effects on the characteristics of heat and mass transfer in the conditions of conjugate natural convection. *J. Eng. Thermophys.* **2010**, *19*, 119–127.
12. Kuznetsov, G.V.; Sheremet, M.A. A numerical simulation of double-diffusive conjugate natural convection in an enclosure. *Int. J. Therm. Sci.* **2011**, *50*, 1878–1886.
13. Kefayati, G.R. Double-diffusive mixed convection of pseudoplastic fluids in a two sided lid-driven cavity using FDLBM. *J. Taiwan Inst. Chem. Eng.* **2014**, *45*, 2122–2139.
14. Kefayati, G.R. Mesoscopic simulation of magnetic field effect on double-diffusive mixed convection of shear-thinning fluids in a two sided lid-driven cavity. *J. Mol. Liq.* **2014**, *198*, 413–429.
15. Bhagat, K.D.; Tripathi, M.K.; Sahu, K.C. Instability due to double-diffusive phenomenon in pressure-driven displacement flow of one fluid by another in an axisymmetric pipe. *Eur. J. Mech. B Fluids* **2016**, *55*, 63–70.
16. Nikbakhti, R.; Rahimi, A.B. Double-diffusive natural convection in a rectangular cavity with partially thermally active side walls. *J. Taiwan Inst. Chem. Eng.* **2012**, *43*, 535–541.
17. Wang, J.; Yang, M.; He, Y.L.; Zhang, Y. Oscillatory double-diffusive convection in a horizontal cavity with Soret and Dufour effects. *Int. J. Therm. Sci.* **2016**, *106*, 57–69.
18. Alvarado-Juárez, R.; Xamán, J.; Álvarez, G.; Hernández-López, I. Numerical study of heat and mass transfer in a solar still device: Effect of the glass cover. *Desalination* **2015**, *359*, 200–211.
19. Bejan, A. *Entropy Generation Minimization: The Method of Thermodynamic Optimization of Finite-Size Systems and Finite-Time Processes*; CRC Press: Boca Raton, FL, USA, 1995.
20. Torabi, M.; Zhang, K. Temperature distribution, local and total entropy generation analyses in MHD porous channels with thick walls. *Energy* **2015**, *87*, 540–554.
21. Torabi, M.; Zhang, K.; Karimi, N.; Peterson, G.P. Entropy generation in thermal systems with solid structures—A concise review. *Int. J. Heat Mass Transf.* **2016**, *97*, 917–931.
22. Magherbi, M.; Abbassi, H.; Hidouri, N.; Brahim Ammar, B. Second law analysis in convective heat and mass transfer. *Entropy* **2006**, *8*, 1–17.
23. Chen, S.; Du, R. Entropy generation of turbulent double-diffusive natural convection in a rectangle cavity. *Energy* **2011**, *36*, 1721–1734.
24. Chen, S.; Yang, B.; Xiao, X.; Zheng, C. Analysis of entropy generation in double-diffusive natural convection of nanofluid. *Int. J. Heat Mass Transf.* **2015**, *87*, 447–463.
25. Matin, M.H.; Khan, W.A. Entropy generation analysis of heat and mass transfer in mixed electrokinetically and pressure driven flow through a slit microchannel. *Energy* **2013**, *56*, 207–217.
26. Oueslati, F.; Ben-Beya, B.; Lili, T. Double-diffusive natural convection and entropy generation in an enclosure of aspect ratio 4 with partial vertical heating and salting sources. *Alexandria Eng. J.* **2013**, *52*, 605–625.
27. Kefayati, G.R. FDLBM simulation of entropy generation in double diffusive natural convection of power-law fluids in an enclosure with Soret and Dufour effects. *Int. J. Heat Mass Transf.* **2015**, *89*, 267–290.
28. Kefayati, G.R. Simulation of double diffusive MHD (magnetohydrodynamic) natural convection and entropy generation in an open cavity filled with power-law fluids in the presence of Soret and Dufour effects (part II: Entropy generation). *Energy* **2016**, *107*, 917–959.
29. Kefayati, G.R. Simulation of double diffusive MHD (magnetohydrodynamic) natural convection and entropy generation in an open cavity filled with power-law fluids in the presence of Soret and Dufour effects (Part I: Study of fluid flow, heat and mass transfer). *Energy* **2016**, *107*, 889–916.
30. Mchirgui, A.; Hidouri, N.; Brahim, A.B.; Magherbi, M. Entropy generation in double-diffusive convection in a square Porous cavity using Darcy-Brinkman formulation. *Transp. Porous Media* **2012**, *93*, 223–240.
31. Mchirgui, A.; Hidouri, N.; Magherbi, M.; Ben Brahim, A. Second law analysis in double diffusive convection through an inclined porous cavity. *Comput. Fluids* **2014**, *96*, 105–115.
32. Hussain, S.H. Analysis of heatlines and entropy generation during double-diffusive MHD natural convection within a tilted sinusoidal corrugated porous enclosure. *Eng. Sci. Technol. Int. J.* **2016**, *19*, 926–945.

33. Kefayati, G.R. Simulation of double diffusive natural convection and entropy generation of power-law fluids in an inclined porous cavity with Soret and Dufour effects (Part II: Entropy generation). *Int. J. Heat Mass Transf.* **2016**, *94*, 582–624.
34. Kefayati, G.R. Simulation of double diffusive natural convection and entropy generation of power-law fluids in an inclined porous cavity with Soret and Dufour effects (Part I: Study of fluid flow, heat and mass transfer). *Int. J. Heat Mass Transf.* **2016**, *94*, 539–581.
35. Torabi, M.; Zhang, Z.; Peterson, G.P. Interface entropy generation in micro porous channels with velocity slip and temperature jump. *Appl. Therm. Eng.* **2017**, *111*, 684–693.
36. Torabi, M.; Peterson, G.P. Effects of velocity slip and temperature jump on the heat transfer and entropy generation in micro porous channels under magnetic field. *Int. J. Heat Mass Transf.* **2016**, *102*, 585–595.
37. Chen, Y.; Shen, C.; Shi, M.; Peterson, G.P. Visualization study of flow condensation in hydrophobic microchannels. *AIChE J.* **2014**, *60*, 1182–1192.
38. Matin, M.H.; Pop, I. Forced convection heat and mass transfer flow of a nanofluid through a porous channel with a first order chemical reaction on the wall. *Int. Commun. Heat Mass Transf.* **2013**, *46*, 134–141.
39. Pallares, J.; Grau, F.X. Mass transfer rate of a first-order chemical reaction on a wall at high Schmidt numbers. *Int. J. Heat Mass Transf.* **2014**, *69*, 438–442.
40. Pallares, J. Local mass transfer rates of a first-order chemical reaction on a wall: Application to the prediction of local platelet deposition in a perfusion chamber. *Int. J. Heat Mass Transf.* **2015**, *90*, 254–258.
41. Torabi, M.; Zhang, K. First and second thermodynamic laws analyses between and inside two rotating solid cylindrical geometries with magnetohydrodynamic flow. *Int. J. Heat Mass Transf.* **2015**, *89*, 760–769.
42. Torabi, M.; Zhang, K.; Yang, G.; Wang, J.; Wu, P. Temperature distribution, local and total entropy generation analyses in asymmetric cooling composite geometries with multiple nonlinearities: Effect of imperfect thermal contact. *Energy* **2014**, *78*, 218–234.
43. Gaffar, S.A.; Prasad, V.R.; Reddy, E.K.; Bég, O.A. Thermal radiation and heat generation/absorption effects on viscoelastic double-diffusive convection from an isothermal sphere in porous media. *Ain Shams Eng. J.* **2015**, *6*, 1009–1030.



© 2017 by the authors. Licensee MDPI, Basel, Switzerland. This article is an open publication under the terms and conditions of the Creative Commons Attribution (CC BY) license (<http://creativecommons.org/licenses/by/4.0/>).